

MAGNETIC EXCITATIONS IN THE TRIMERIC COMPOUNDS

$A_3Cu_3(PO_4)_4$ ($A = Ca, Sr, Pb$)

M. Georgiev and H. Chamati

Abstract

We study the magnetic excitations of the trimeric magnetic compounds $A_3Cu_3(PO_4)_4$ ($A = Ca, Sr, Pb$). The spectra are analyzed in terms of the Heisenberg model and a generic spin Hamiltonian that accounts for the changes in valence electrons distribution along the bonds among magnetic ions. The analytical results obtained in the framework of both Hamiltonians are compared to each other and to the available experimental measurements. The results based on our model show better agreement with the experimental data than those obtained with the aid of the Heisenberg model. For all trimers, our analysis reveals the existence of one thin energy band referring to the flatness of observed excitation peaks.

1 Introduction

Molecular magnets possess unique properties and are ideal candidates for exploring the interplay of the quantum and the classical worlds. They may manifest a great variety of magnetic features determined from weakly interacting isolated fundamental structural units, such as dimers, trimers and tetramers^[1]. The effect of quantum tunneling in single-molecule magnets^[2,3] and the response of spin-switching in the frustrated antiferromagnetic chromium trimer^[4] are some prominent examples. With their short-range spin correlation the small spin clusters stand as elegant tools for studying the relevant coupling processes. Magnetic measurements on trimer copper chains $A_3Cu_3(PO_4)_4$ with ($A = Ca, Sr$), reported in Ref.^[5], show that the intertrimer exchange couplings are negligible and thus the trimers might be considered as separate clusters. These results were confirmed via INS experiments^[6,7] that shed light on the magnetic spectra with the aid of the antiferromagnetic Heisenberg model involving nearest and next-nearest intratrimer interactions, and later they were extended to the compound $Ca_3Cu_3(PO_4)_4$ ^[1]. Moreover, it turns out that the interaction between edged spins in isolated trimers is also negligible. The difference in the magnetic properties among the compounds $Ca_3Cu_2Ni(PO_4)_4$ ^[8] and $Ca_3Cu_2Mg(PO_4)_4$ ^[9] is another demonstration for the richness of the physical features arising from a symmetrically trivial linear spin trimers, see e.g. Ref.^[10].

In the present article we report a theoretical study of the magnetic spectra of magnetic clusters. We focus our attention on the trimeric compounds $A_3Cu_3(PO_4)_4$ with ($A = Ca, Sr, Pb$), for which the magnetic excitations are determined experimentally^[6,7]. To describe the magnetism in the compounds $A_3Cu_3(PO_4)_4$ we employ the approach devised in Refs.^[11,12]. The approach is based on a generic spin Hamiltonian that allows to compute effectively the changes of electron's density distribution along the complex exchange bridges among magnetic centers. We compare the results of our study obtained in the framework of the named generic spin Hamiltonian and its Heisenberg counterpart demonstrating their equivalence and differences.

The rest of this paper is structured as follows: In Section 2 we present the keystone relations for the neutron scattering intensities and formulate explicitly the generic spin Hamiltonian. In Sections 3 we explore the low-lying magnetic excitations of the compounds $A_3Cu_3(PO_4)_4$ (where A stands for Ca, Sr, Pb) within the framework of the Heisenberg model and our Hamiltonian. A summary of the results obtained throughout this paper along with conclusions are presented in Section 4.

2 The model and the method

2.1 Inelastic Neutron Scattering

To determine the energy level structure and the transitions corresponding to the experimentally observed magnetic spectra one needs a number of parameters to account for all couplings in the system. It is cumbersome to apply a general approach with a unique set of parameters that can describe all possible magnetic effects and in addition to distinguish between inter-molecular and intra-molecular features. Usually, one starts with bilinear spin microscopic models, such as the Heisenberg Hamiltonian^[13] and depending on the exhibited magnetic features different interaction terms are included^[14].

To obtain meaningful results one calculates the neutron scattering intensities $I_{n'n}(\mathbf{q})$ integrated over the angles of scattering vector \mathbf{q} of the neutron. For identical magnetic ions, represented by the operators \hat{s}_i^α and \hat{s}_j^β , they read^[15–18]

$$I_{n'n}(\mathbf{q}) \propto F^2(\mathbf{q}) \sum_{\alpha,\beta} \Theta^{\alpha\beta} S^{\alpha\beta}(\mathbf{q}, \omega_{n'n}), \quad (1)$$

where $F(\mathbf{q})$ is the spin magnetic form factor^[19], $\Theta^{\alpha\beta}$ is the polarization factor and $\alpha, \beta, \gamma \in \{x, y, z\}$. In (1) the magnetic scattering functions are explicitly written as

$$S^{\alpha\beta}(\mathbf{q}, \omega_{n'n}) = \sum_{n,n',i,j} e^{i\mathbf{q}\cdot\mathbf{r}_{ij}} p_n \langle n | \hat{s}_i^\alpha | n' \rangle \langle n' | \hat{s}_j^\beta | n \rangle \delta(\hbar\omega_{n'n} - E_{n'n}), \quad (2)$$

where $\omega_{n'n}$ is the frequency of a magnetic excitation related to a transition between the states $|n\rangle$ and $|n'\rangle$ with the corresponding energy E_n and $E_{n'}$, respectively. Further, $e^{i\mathbf{q}\cdot\mathbf{r}_{ij}}$ is the structure factor associated with the cluster geometry, $p_n = Z^{-1}e^{-E_n/k_B T}$ is the population factor (with Z the partition function).

2.2 The generic spin model

The distribution of coupled magnetic centers (ions) plays a crucial role in uniquely determining the scattering intensities. Even when these effective bonds are indistinguishable with respect to their lengths and the total spin, according to (2), one can obtain different in magnitude neutron scattering intensities. However, to identify each intensity one has to use an appropriate spin model leading to an energy sequence such that the δ function in the r.h.s of (2) defines the relevant spin bonds with respect to the structure factors.

To describe the magnetic spectra in the considered trimeric compounds we employ the proposed in Ref.^[11,12] generic spin Hamiltonian

$$\hat{\mathcal{H}} = \sum_{i \neq j} J_{ij} \hat{\sigma}_i \cdot \hat{\sigma}_j, \quad (3)$$

where the couplings $J_{ij} = J_{ji}$ are effective exchange constants and the operator $\hat{\sigma}_i \equiv (\hat{\sigma}_i^x, \hat{\sigma}_i^y, \hat{\sigma}_i^z)$ accounts for the differences in valence electron's distribution with respect to the i th magnetic center. Let us note that model (3) was applied successfully to explore the magnetic spectra of the molecular magnet $\text{Ni}_4\text{Mo}_{12}$ ^[12].

3 Magnetic spectra of the trimers $\text{A}_3\text{Cu}_3(\text{PO}_4)_4$ (A = Ca, Sr and Pb)

3.1 The Hamiltonian

The magnetic compounds $\text{A}_3\text{Cu}_3(\text{PO}_4)_4$ (A = Ca, Sr, Pb) are convenient spin trimer systems for testing the Hamiltonian (3). On Fig. 1 (a) we show a small fragment of the copper ions structure with the relevant exchange pathways with respect to the arrangement of oxygen atoms. Whence the Cu2 ion is surrounded by four oxygen atoms on a plane, while Cu1 and Cu3 ions are surrounded by five oxygen atoms constructing a distorted square pyramid. For the sake of clarity the other elements are not shown and only two oxygen atoms along the intratrimer Cu1–O1–Cu2 and intertrimer Cu2–O2–Cu4 pathways are labeled. In general, the exchange processes appear to be more complex and depend on the global structure of the compounds^[5]. Besides the superexchange interactions are sensitive^[6] to the angle between Cu^{2+} bonds and their lengths suggesting that the intertrimer Cu2–Cu4 interaction is much smaller than the intratrimer ones, *i.e.* Cu1–Cu2 and Cu3–Cu2. Thus, the intertrimer exchange can be neglected and the Cu^{2+} sub-lattice is considered as a one-dimensional array of isolated spin trimers Fig. 1 (b).

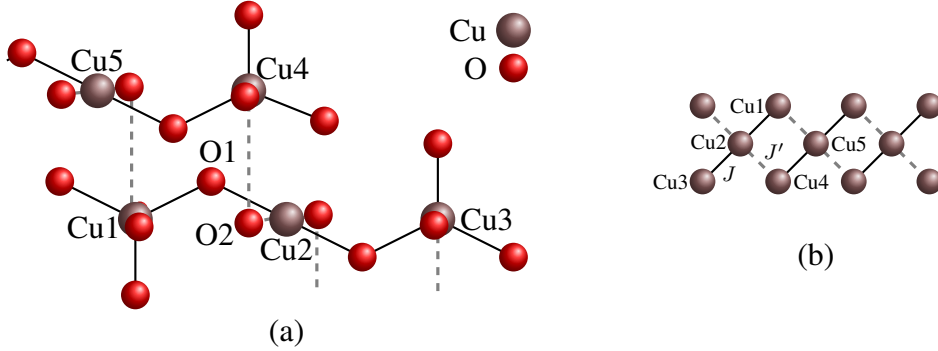


Figure 1: (a) Exchange pathways in $\text{A}_3\text{Cu}_3(\text{PO}_4)_4$ (A = Ca, Sr, Pb). Copper colored circles represent copper ions, the red ones stand for oxygen atoms. The solid (black) and dashed (gray) lines represent the intratrimer and intertrimer exchange pathways, respectively. (b) Schematic representation of the intratrimer J and intertrimer J' magnetic interactions in the array of isolated trimers.

Taking into account that Cu1-Cu2 and Cu2-Cu3 are bonded by a single oxygen ion we set $J_{ij} \rightarrow J_{12} = J$ and perform a study of the magnetic excitations. Owing to the trimer symmetry we apply the coupling scheme $|s_2 - s_{13}| \leq s \leq |s_2 + s_{13}|$, where s and s_{13} (with $|s_1 - s_3| \leq s_{13} \leq |s_1 + s_3|$) are the trimer and Cu1-Cu3 coupled pair spin quantum numbers, respectively. Thus, the Hamiltonian (3) reads

$$\hat{\mathcal{H}} = J (\hat{\sigma}_{13} \cdot \hat{s}_2 + \hat{\sigma}_2 \cdot \hat{s}_{13} + \hat{\sigma}_1 \cdot \hat{s}_3 + \hat{\sigma}_3 \cdot \hat{s}_1). \quad (4)$$

With respect to the selected spin coupling scheme the total spin eigenstates are denoted by $|s_{13}, s, m\rangle$.

3.2 Energy levels

The isolated trimer is described by four quartet and four doublet eigenstates. The eigenvalues of (4) are denoted by $E_{s_{13},s}^m$. Further, analyzing the energy spectrum we obtain the ground state energy for $s_{13} = 1, s = \frac{1}{2}$. The respective doublet states are $|1, \frac{1}{2}, \pm \frac{1}{2}\rangle$ with corresponding energies

$$E_{1,1/2}^{\pm 1/2} = -\frac{3}{2}J. \quad (5)$$

The second pair of doublet states is associated with the first excited energy level, see Fig. 2. The edged spins of the isolated trimer are coupled in a singlet, with corresponding state $|0, \frac{1}{2}, \pm \frac{1}{2}\rangle$. Now, using (4) we end up with

$$E_{0,1/2}^{\pm 1/2} = -\frac{3}{2}Ja_{13}^{0,0}, \quad (6)$$

where the parameter $a_{13}^{0,0} \in \mathbb{R}$ account for the variations of electrons spatial distribution along the Cu1-Cu3 exchange bridge. To fully characterize the experimentally observed transitions for $\text{Pb}_3\text{Cu}_3(\text{PO}_4)_4$ one requires at least three excited energy levels. Bearing in mind that the quartet level is four-fold degenerate, we deduce that the corresponding coefficient may take only two values $a_{13}^{0,0} \in \{c_{13}^1, c_{13}^2\}$. Further, the observed excitations spectra^[6] are not broadened signaling that $|c_{13}^1 - c_{13}^2| \approx 0$. Therefore, taking into account (6) we get

$$E_{0,1/2}^{\pm 1/2} = -\frac{3}{2}Jc_{13}^n \quad n = 1, 2.$$

For all four quartet eigenstates $|1, \frac{3}{2}, m\rangle$, with $m = \pm \frac{1}{2}, \pm \frac{3}{2}$, we have

$$E_{1,3/2}^{\pm 1/2} = E_{1,3/2}^{\pm 3/2} = \frac{3}{2}J.$$

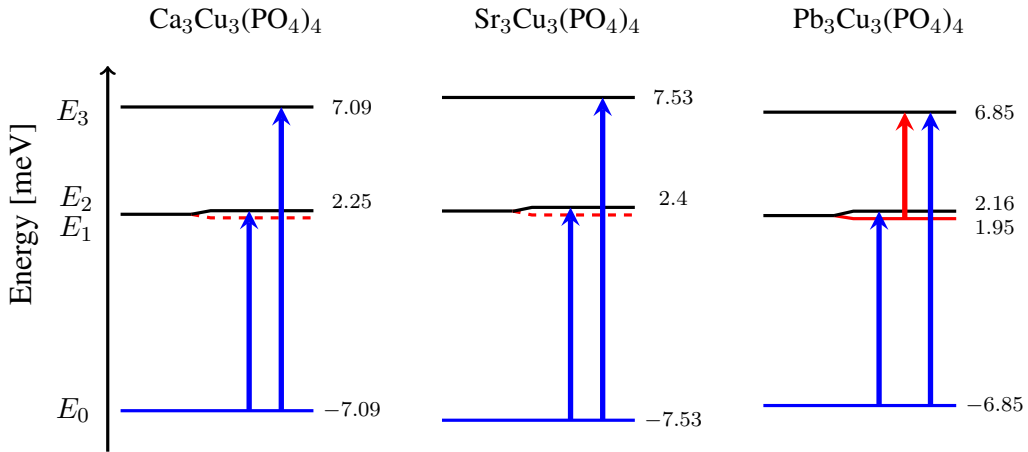


Figure 2: Energy level structure of the compounds $\text{A}_3\text{Cu}_3(\text{PO}_4)_4$ ($\text{A} = \text{Ca}, \text{Sr}, \text{Pb}$). The blue arrows show the ground state transitions, while the red arrow stands for the excited transition. The energy levels corresponding to the ground state are designated by blue lines. The initial energy level of the excited transition is depicted by a red line, while by analogy to $\text{Pb}_3\text{Cu}_3(\text{PO}_4)_4$ the dashed red lines stand for a presumed second sub level of the excited doublet level.

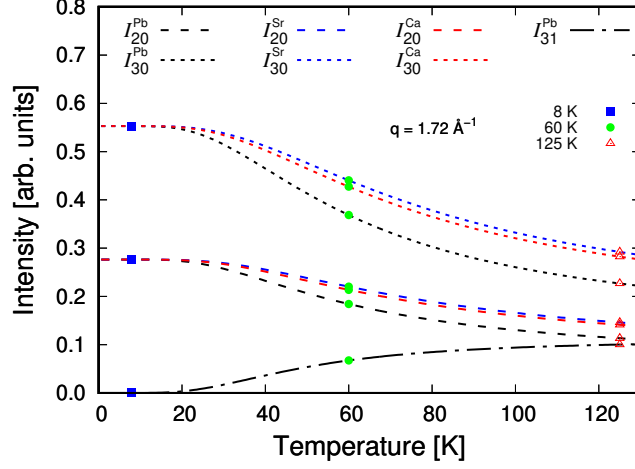


Figure 3: Scattering intensities I_{20}^A , I_{30}^A and I_{31}^{Pb} with ($A = \text{Ca, Sr, Pb}$) as a function of the temperature, calculated with the Hamiltonian (3). The blue squares, the green circles and red triangles correspond to the values of the intensities given in Tab. 2.

The energy sequence consists of four levels. Henceforth we denote these levels as follow

$$E_0 = -\frac{3}{2}J, \quad E_1 = -\frac{3}{2}Jc_{13}^1, \quad E_2 = -\frac{3}{2}Jc_{13}^2, \quad E_3 = \frac{3}{2}J. \quad (7)$$

Therefore, we have at hand the parameters J and c_{13}^n . The coupling J accounts for the interaction along Cu1-Cu2 and Cu2-Cu3 bridges and c_{13}^n will indicate any changes in the interaction between edged ions. However, we take further actions and derive the following relation $Jc_{13}^n = J(\frac{3}{4}c_{13}^n + \frac{1}{4})$, where Jc_{13}^n represents the exchange constant between the next-nearest neighbors.

3.3 Scattering intensities

Based on the selection rules $\Delta s_{13} = 0, \pm 1$, $\Delta s = 0, \pm 1$ and $\Delta m = 0, \pm 1$ and the aid of the identities $S^{\alpha\beta}(\mathbf{q}, \omega_{n'n}) + S^{\beta\alpha}(\mathbf{q}, \omega_{n'n}) = 0$, $S^{\alpha\alpha}(\mathbf{q}, \omega_{n'n}) = S^{\beta\beta}(\mathbf{q}, \omega_{n'n})$, where $\alpha \neq \beta$ and $n, n' = 0, 1, 2, 3$, we may compute the scattering functions. Moreover, taking into account the cluster structure, we have $\sum_{\alpha} \Theta^{\alpha\alpha} = 2$. The analysis of intensities reported in^[6] allows us to determine the observed first magnetic excitation. It corresponds to the transition between the ground state energy E_0 and E_2 with scattering functions

$$S^{\alpha\alpha}(\mathbf{q}, \omega_{20}) = \frac{1}{3}[1 - \cos(2\mathbf{q} \cdot \mathbf{r})]p_0,$$

where \mathbf{r} is the vector of the average distance r between neighboring ions with $\mathbf{r}_{31} = 2\mathbf{r}$. The degeneracy of the quartet energy level is four-fold and hence the second ground state excitation refers to transition from the doublet $|1, \frac{1}{2}, \pm \frac{1}{2}\rangle$ to the quartet states $|1, \frac{3}{2}, m\rangle$, where $m = \pm \frac{1}{2}, \pm \frac{3}{2}$. Hence, for $E_0 \rightarrow E_3$ we get

$$S^{\alpha\alpha}(\mathbf{q}, \omega_{30}) = \frac{2}{9}[3 + \cos(2\mathbf{q} \cdot \mathbf{r}) - 4 \cos(\mathbf{q} \cdot \mathbf{r})]p_0.$$

The excited peak is indicated by the transition $E_1 \rightarrow E_3$. The corresponding scattering functions are

$$S^{\alpha\alpha}(\mathbf{q}, \omega_{31}) = \frac{2}{3}[1 - \cos(2\mathbf{q} \cdot \mathbf{r})]p_1.$$

Therefore, according to (1) we estimate the relevant intensities obtaining

$$\begin{aligned} I_{20} &\propto \gamma_{20} \left[1 - \frac{\sin(2qr)}{2qr} \right] F^2(q), & I_{30} &\propto \gamma_{30} \left[1 + \frac{\sin(2qr)}{6qr} - 4 \frac{\sin(qr)}{3qr} \right] F^2(q), \\ I_{31} &\propto \gamma_{31} \left[1 - \frac{\sin(2qr)}{2qr} \right] F^2(q), \end{aligned} \quad (8)$$

where $\gamma_{20} = \frac{2}{3}p_0$, $\gamma_{30} = \frac{12}{9}p_0$ and $\gamma_{31} = \frac{4}{3}p_1$. Moreover, for dications Cu^{2+} the form factor reads $F(q) = 256/(16 + q^2 r_o^2)^2$, where q is the magnitude of the scattering vector, $r_o = 0.529 \text{ \AA}$ is the Bohr radius.

3.4 Energy of the magnetic transitions

Taking into account (7) and (8) for the transition energies we get

$$E_{20} = \frac{3}{2}J(1 - c_{13}^2), \quad E_{30} = 3J, \quad E_{31} = \frac{3}{2}J(1 + c_{13}^2). \quad (9)$$

Neutron scattering experiments performed on $\text{Pb}_3\text{Cu}_3(\text{PO}_4)_4$ with $T \geq 60 \text{ K}$ ^[6] show the presence of a third peak at about 4.9 meV, which may be related to the excited transition energy E_{31} . The values of c_{13}^1 , c_{13}^2 and J , according to INS experiments^[6] performed on polycrystalline samples $\text{A}_3\text{Cu}_3(\text{PO}_4)_4$ ($\text{A} = \text{Ca}, \text{Sr}, \text{Pb}$) are shown in Tab. 1. In addition, for the compound $\text{Ca}_3\text{Cu}_3(\text{PO}_4)_4$ we have $c_{13}^2 = -0.32(8)$ and $J \approx 4.741 \text{ meV}$ based on INS data at $T = 1.5 \text{ K}$ ^[7,13].

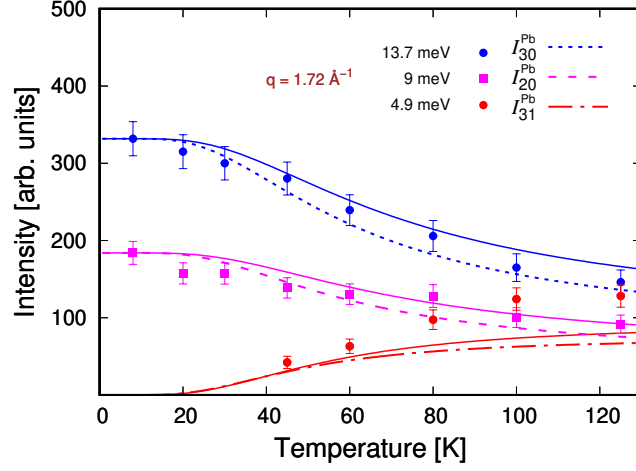
Table 1: The values of the coupling constants and the quantities c_{13}^1 , c_{13}^2 for our model applied to $\text{A}_3\text{Cu}_3(\text{PO}_4)_4$ ($\text{A} = \text{Ca}, \text{Sr}, \text{Pb}$) obtained by taking into account the experimental data in Ref.^[6].

A	E_{20}	E_{30}	E_{31}	c_{13}^1	c_{13}^2	J	$J_{c_{13}^2}$	$J_{c_{13}^1}$
Ca	9.335	14.174	—	—	-0.317	4.725	0.058	—
Sr	9.936	15.064	—	—	-0.319	5.021	0.054	—
Pb	9.005	13.693	4.9	-0.284	-0.315	4.564	0.062	0.168

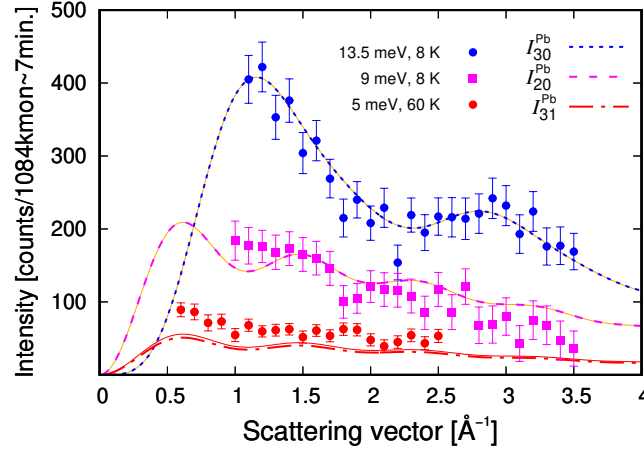
The temperature dependence of the integrated scattering intensities for each compound is shown on Fig. 3. On Fig. 4a we present the scattering intensities for $\text{Pb}_3\text{Cu}_3(\text{PO}_4)_4$ computed with our Hamiltonian and the Heisenberg model along with the experimental data taken from Ref.^[6]. Let us point out that our results are in better agreement with their experimental counterpart for I_{20}^{Pb} and I_{30}^{Pb} , while for I_{31}^{Pb} we have a qualitative agreement. The averaged magnitudes of the scattering vector q and the distance r between neighboring ions are taken from Ref.^[6], $q = 1.72 \text{ \AA}^{-1}$ and $r = 3.6 \text{ \AA}$. The explicit expressions of the scattering intensities for each transition are

$$I_{20}^{\text{A}}(T) \propto 0.5528 Z_{\text{A}}^{-1} e^{-\frac{E_0^{\text{A}}}{k_B T}}, \quad I_{30}^{\text{A}}(T) \propto 1.1057 Z_{\text{A}}^{-1} e^{-\frac{E_0^{\text{A}}}{k_B T}}, \quad I_{31}^{\text{Pb}}(T) \propto 1.1056 Z_{\text{Pb}}^{-1} e^{-\frac{E_1^{\text{Pb}}}{k_B T}}, \quad (10)$$

where $\text{A} = \text{Ca}, \text{Sr}, \text{Pb}$. As T vanishes the scattering intensities I_{20}^{A} and I_{30}^{A} are equal by about a factor of 2, see Tab. 2. For $T > 20 \text{ K}$ a third peak sets in, but the evaluated intensity I_{31}^{Pb} remains smaller than the experimentally observed one^[6]. In contrast to the functions I_{30}^{Pb} and I_{20}^{Pb} the intensities of the ground state transitions for $\text{A} = \text{Ca}, \text{Sr}$ decrease slowly with temperature. The predicted



(a) Scattering intensities for the compound $\text{Pb}_3\text{Cu}_3(\text{PO}_4)_4$ as a function of the temperature, along with experimental results from Ref. [6]. The solid and dashed lines show the calculated intensities for the Heisenberg model and Hamiltonian (3), respectively.



(b) Calculated intensities as a function of the scattering vector for $\text{Pb}_3\text{Cu}_3(\text{PO}_4)_4$ along with the experimental data of Ref. [6]. The dashed lines depict the intensities obtained from the Hamiltonian (3). The solid red and orange lines correspond to the Heisenberg model. I_{20}^{Pb} and I_{30}^{Pb} correspond to the ground state transitions at $T = 8$ K. The intensity I_{31}^{Pb} stands for the excited transition at $T = 60$ K.

Figure 4: Scattering intensities.

peak for $\text{Pb}_3\text{Cu}_3(\text{PO}_4)_4$ is in concert with the experimental findings [6]. Unfortunately there are no experimental data confirming the presence of this third peak for the compounds $\text{Ca}_3\text{Cu}_3(\text{PO}_4)_4$ and $\text{Sr}_3\text{Cu}_3(\text{PO}_4)_4$ and hence the energy level E_1 could not be included in determining the sequence of energy spectrum. On Fig. 2 the presumed energy levels E_1^{Ca} and E_1^{Sr} are illustrated with dashed red lines. For all compounds the scattering intensities as a function of the magnitude of the scattering vector are represented in Fig. 4b.

Table 2: Calculated values of integrated scattering intensities $I_{n'n}^A$ [arb. units], using the Hamiltonian (3), for the trimers $A_3Cu_3(PO_4)_4$ ($A = Ca, Sr, Pb$) at temperatures 8, 60 and 125 K, depicted on Fig. 3.

T [K]	8	60	125
I_{20}^{Ca}	0.276(4)	0.213(7)	0.141(2)
I_{30}^{Ca}	0.552(8)	0.427(4)	0.282(5)
I_{20}^{Sr}	0.276(4)	0.220(2)	0.146(1)
I_{30}^{Sr}	0.552(8)	0.440(5)	0.292(2)
I_{20}^{Pb}	0.276(4)	0.184(3)	0.113(4)
I_{30}^{Pb}	0.552(8)	0.368(6)	0.226(8)
I_{31}^{Pb}	0	0.067(3)	0.100(3)

4 Conclusion

We propose an study for the magnetic excitations of the compounds $A_3Cu_3(PO_4)_4$ with ($A = Ca, Sr, Pb$). To this end, we use a generic bilinear spin Hamiltonian (3) that accounts for the variations in the electron's spatial distributions along the exchange bridges. Alongside with the named Hamiltonian we compute the magnetic spectrum in the framework of the Heisenberg Hamiltonian and compare the outcome from both models, see Figs. 4a and 4b. We found that the results obtained with our model are in better agreement with the INS experimental data^[6,7] than the Heisenberg model. On the other hand our results for the Heisenberg model coincide with those reported by other authors^[6,7,13].

With respect to the energy levels sequence and relevant eigenstates the Heisenberg and our Hamiltonian (3) lead to similar values. For the investigated compounds, the ground state energy is related to the Cu1-Cu3 triplet bond, and the neutron energy loss, associated to both ground state magnetic excitations, is due to the local triplet-singlet transition. However, the spin Hamiltonian (4), with the intrinsic parameter $a_{13}^{0,0}$, identifies the experimentally observed third peak (about 4.9 meV) for the compound $Pb_3Cu_3(PO_4)_4$ ^[6] accurately, while the Heisenberg model is unable to reproduce it. We obtain one thin energy band composed of two very close energy levels that corresponds to the Cu1-Cu3 singlet state (see e.g. Fig. 2). The energy band width signals for the small change in the electrons distribution along the Cu1-Cu2-Cu3 bridge due to the temperature. Thus, the intensities indicated by dashed lines on Fig. 4a decrease rapidly than in the case of the Heisenberg model. In other words, the inequality $|c_{13}^n| < 1$ for $n = 1, 2$, shows that in the doublet level, the spatial distribution of the electrons common to the edge ions is such that the exchange becomes negligible. Further, it points out that the next-nearest neighbor coupling slightly varies with respect to the temperature taking two values $J_{13} \in \{J_{c_{13}^1}, J_{c_{13}^2}\}$, see Tab. 1. On the other hand the difference $|c_{13}^1 - c_{13}^2| = 0.031$ explains the sharpness of the experimentally observed peaks^[6,7].

Acknowledgments

The authors are indebted to Prof. N. Ivanov and Prof. J. Schnack for very helpful discussions, and to Prof. M. Matsuda for providing us with the experimental data used in FIGs. 4a and 4b. This work was supported by the Bulgarian National Science Fund under contract DN/08/18.

References

- [1] A. Furrer and O. Waldmann, “Magnetic cluster excitations,” *Rev. Mod. Phys.* **85**, 367 (2013).
- [2] W. Wernsdorfer, N. Aliaga-Alcalde, D. N. Hendrickson, and G. Christou, “Exchange-biased quantum tunnelling in a supramolecular dimer of single-molecule magnets,” *Nature* **416**, 406 (2002).
- [3] R. Schenker, M. N. Leuenberger, G. Chaboussant, D. Loss, and H. U. Güdel, “Phonon bottleneck effect leads to observation of quantum tunneling of the magnetization and butterfly hysteresis loops in $(\text{Et}_4\text{N})_3\text{Fe}_2\text{F}_9$,” *Phys. Rev. B* **72**, 184403 (2005).
- [4] T. Jamneala, V. Madhavan, and M. Crommie, “Kondo Response of a Single Antiferromagnetic Chromium Trimer,” *Phys. Rev. Lett.* **87**, 256804 (2001).
- [5] M. Drillon, M. Belaiche, P. Legoll, J. Aride, A. Boukhari, and A. Moqine, “1D ferrimagnetism in copper(II) trimetric chains: Specific heat and magnetic behavior of $\text{A}_3\text{Cu}_3(\text{PO}_4)_4$ with $\text{A} = \text{Ca, Sr}$,” *J. Magnet. Magnet. Mater.* **128**, 83 (1993).
- [6] M. Matsuda, K. Kakurai, A. A. Belik, M. Azuma, M. Takano, and M. Fujita, “Magnetic excitations from the linear Heisenberg antiferromagnetic spin trimer system $\text{A}_3\text{Cu}_3(\text{PO}_4)_4$ ($\text{A} = \text{Ca, Sr, and Pb}$),” *Phys. Rev. B* **71**, 144411 (2005).
- [7] A. Podlesnyak, V. Pomjakushin, E. Pomjakushina, K. Conder, and A. Furrer, “Magnetic excitations in the spin-trimer compounds $\text{Ca}_3\text{Cu}_{3-x}\text{Ni}_x(\text{PO}_4)_4$ ($x = 0, 1, 2$),” *Phys. Rev. B* **76**, 064420 (2007).
- [8] M. Ghosh and K. Ghoshray, “Spin trimers in $\text{Ca}_3\text{Cu}_2\text{Ni}(\text{PO}_4)_4$,” *Low Temp. Phys.* **38**, 645 (2012).
- [9] M. Ghosh, M. Majumder, K. Ghoshray, and S. Banerjee, “Magnetic properties of the spin trimer compound $\text{Ca}_3\text{Cu}_2\text{Mg}(\text{PO}_4)_4$ from susceptibility measurements,” *Phys. Rev. B* **81**, 094401 (2010).
- [10] M. Ghosh, K. Ghoshray, M. Majumder, B. Bandyopadhyay, and A. Ghoshray, “NMR study of a magnetic phase transition in $\text{Ca}_3\text{CuNi}_2(\text{PO}_4)_4$: A spin trimer compound,” *Phys. Rev. B* **81**, 064409 (2010).
- [11] M. Georgiev and H. Chamati, “Magnetic exchange in spin clusters,” , 020004 (2019).
- [12] M. Georgiev and H. Chamati, “Magnetic excitations in molecular magnets with complex bridges: The tetrahedral molecule $\text{Ni}_4\text{Mo}_{12}$,” *EPJ B (The European Physical Journal B)* (2019), accepted.
- [13] A. Furrer, “Magnetic cluster excitations,” *Int. J. Mod. Phys. B* **24**, 3653 (2010).
- [14] H. Chamati, “Theory of Phase Transitions: From Magnets to Biomembranes,” *Adv. Planar Lipid Bilayers Liposomes* **17**, 237 (2013).
- [15] S. W. Lovesey, *Theory of Neutron Scattering from Condensed Matter: Polarization Effects and Magnetic Scattering*, International Series of Monographs on Physics, Vol. 2 (Oxford University Press, Oxford, New York, 1986).
- [16] M. F. Collins, *Magnetic critical scattering*, Oxford Series on Neutron Scattering in Condensed Matter (Oxford University, New York, 1989).
- [17] A. Furrer, J. Mesot, and T. Strässle, *Neutron Scattering in Condensed Matter Physics*, Series on Neutron Techniques and Applications (World Scientific, 2009).
- [18] B. P. Toperverg and H. Zabel, “Neutron Scattering in Nanomagnetism,” in *Neutron Scattering - Magnetic and Quantum Phenomena*, Experimental Methods in the Physical Sciences, Vol. 48,

edited by F. Fernandez-Alonso and D. L. Price (Elsevier, 2015) p. 339.

[19] J. Jensen and A. R. Mackintosh, *Rare Earth Magnetism : Structures and Excitations*, International Series of Monographs on Physics, Vol. 81 (Clarendon, Oxford; New York, 1991).

Institute of Solid State Physics,
Bulgarian Academy of Sciences,
Tsarigradsko Chaussée 72,
1784 Sofia, Bulgaria
mgeorgiev@issp.bas.bg